An Experimental Study of Chilton–Colburn Analogy Between Turbulent Flow and Convective Heat Transfer of Supercritical Kerosene

Yongjiang Zhang
State Key Laboratory of High Temperature Gas Dynamics,
Institute of Mechanics,
Chinese Academy of Sciences,
Bei-Si-Huan-Xi Road #15,
Beijing 100190, China
e-mail: yongjiang1987@126.com

Fengquan Zhong[1]
State Key Laboratory of High Temperature Gas Dynamics,
Institute of Mechanics,
Chinese Academy of Sciences,
Bei-Si-Huan-Xi Road #15,
Beijing 100190, China;
School of Engineering Science,
University of Chinese Academy of Sciences,
Beijing 100049, China
e-mail: fzhong@imech.ac.cn

Yunfei Xing
State Key Laboratory of High Temperature Gas Dynamics,
Institute of Mechanics,
Chinese Academy of Sciences,
Bei-Si-Huan-Xi Road #15,
Beijing 100190, China
e-mail: xingyunfei@imech.ac.cn

Xinyu Zhang
State Key Laboratory of High Temperature Gas Dynamics,
Institute of Mechanics,
Chinese Academy of Sciences,
Bei-Si-Huan-Xi Road #15,
Beijing 100190, China;
School of Engineering Science,
University of Chinese Academy of Sciences,
Beijing 100049, China
e-mail: changxy@imech.ac.cn

In this paper, characteristics of turbulent flow and convective heat transfer of supercritical China RP-3 kerosene in a horizontal straight circular tube are studied experimentally, and the validity of Chilton–Colburn analogy is examined. Using a three-stage heating system, experiments are conducted at a fuel temperature range of 650–800 K, a pressure range of 3–4 MPa, and a Reynolds number range of 1×10^5–3.5×10^5. The Nusselt number and skin friction coefficient are calculated through control volume analysis proposed in this paper. Heat transfer enhancement and deterioration were observed in the experiments as well as the similar change of skin friction coefficient. The present results show that Chilton–Colburn analogy is also valid for turbulent flow and heat transfer of supercritical kerosene in horizontal straight circular tubes. [DOI: 10.1115/1.4035708]

Keywords: aviation kerosene, supercritical, skin friction coefficient, convective heat transfer, Chilton–Colburn analogy

1 Introduction

Thermal protection is always a critical issue for air-breathing or rocket engine applications. The regenerative cooling technology using on-board hydrocarbon fuels as coolant has been considered as one of the most effective cooling methods [1]. Prior to injection into the combustor, hydrocarbon fuel flows through cooling channels in the combustor wall and absorbs heat via convective heat transfer and endothermicity of fuel pyrolysis [2–4]. Therefore, characteristics of flow and heat transfer of hydrocarbon fuel are the most important and fundamental problems for optimization of regenerative cooling system. In regenerative cooling system, the fuel is often operated at supercritical state and it has relatively large density similar to liquid and gaslike transport properties [5]. More importantly, thermophysical and transport properties of supercritical fuel, such as density and specific heat, exhibit significant variation near the critical temperature and the pseudocritical temperature [5]. All these above features lead to significant differences in flow and heat transfer properties compared to those of simple liquids or gases. For example, many studies have reported that supercritical fluids have heat transfer enhancement or deterioration under certain flow conditions [6,7], and classical heat transfer formulas, such as Dittus–Boelter or Sieder–Tate formulas [8], are not valid and need modifications.

It is known that Chilton–Colburn analogy [9], based on the principle of Reynolds analogy, reveals the relationship between momentum, heat, and mass transfer for fully developed turbulent flows. Relationship between heat and momentum transfer is

$$\mathrm{Nu}/(C_f \mathrm{Pr}^{1/3}) = 0.5\mathrm{Re}_d \tag{1}$$

where Nu is the Nusselt number, C_f is the skin friction coefficient, Pr is the Prandtl number, and Re_d is the Reynolds number defined by tube inner diameter.

Chilton–Colburn analogy has been demonstrated to be valid for the common fluids, such as water or air. Since there is significant difference in heat transfer between simple fluid and supercritical fluid, it is necessary to research whether Chilton–Colburn analogy relation applies to supercritical fuel or not. In this paper, turbulent flow and heat transfer characteristics of supercritical kerosene in a straight, horizontal circular tube are studied experimentally. The Chilton–Colburn analogy relation between turbulent flow and heat transfer is then examined.

2 Experimental Facility

A three-stage heating facility was used to conduct heat transfer experiments. Figure 1 is the schematic diagram of the three-stage heating system. The facility consists of a two-stage preheating device, a test section, a water cooling system, a nitrogen gas driven system, and temperature and pressure measurements. Flow conditions of the test section at a pressure range of 1–5 MPa, a fuel mass flow rate range of 10–50 g/s, and a fuel temperature range of 300–800 K can be achieved. More details of the heating facility can be found in our previous study [3,4].

Figure 2 is the schematic diagram of the test section which is heated by heating taps with a total heating power of 3 kW and insulated by asbestos. The test section is a 2 -m long stainless steel circular tube with an inner diameter of 6 mm. During test runs, wall heat flux increases gradually along the axial distance and its distribution is obtained via measurements of fuel temperature and control volume analysis as addressed in Sec. 3. Four spot-welded K-type thermocouples are used to measure the tube wall temperature and at the same downstream locations, four K-type sheath

[1]Corresponding author.

Contributed by the Heat Transfer Division of ASME for publication in the Journal of Heat Transfer. Manuscript received September 29, 2015; final manuscript received December 22, 2016; published online February 28, 2017. Assoc. Editor: Debjyoti Banerjee.

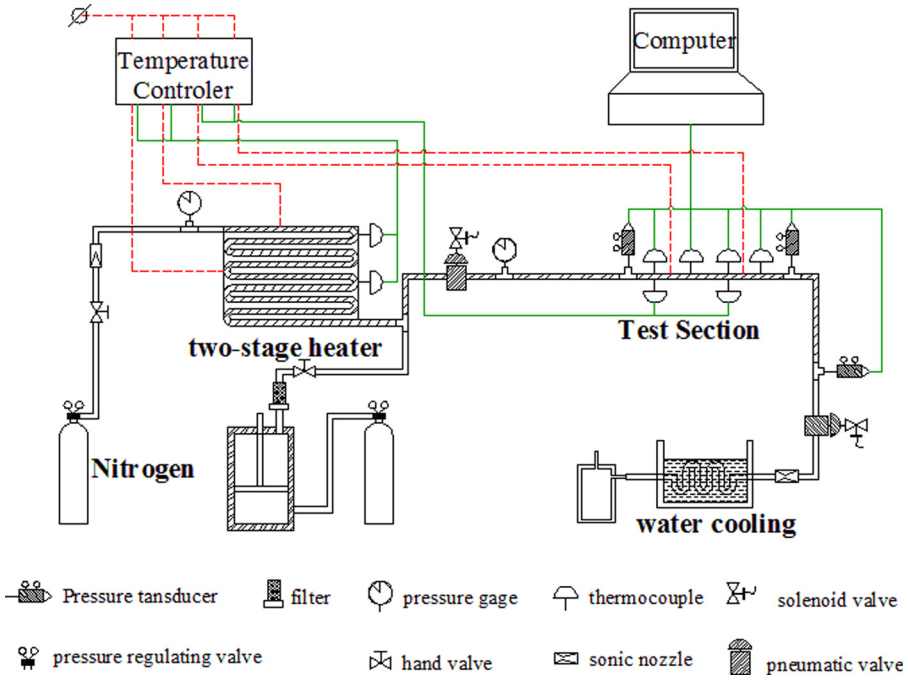

Fig. 1 Schematic diagram of the three-stage heating facility

thermocouples are installed to measure the fuel temperature in the same way that is used in our previous experiments [4]. The uncertainty of the thermocouple measurement is found to be less than ±3 K. Pressure drop between each two adjacent axial locations is measured by high-resolution differential pressure sensor with an uncertainty of less than 100 Pa. The pressure and temperature at the inlet and outlet of the test section are also measured by pressure sensors and thermocouples. A sonic nozzle flow meter was used to control and measure the mass flow rate at the outlet of the test section as described in detail in our previous studies [3], and a measurement error of approximately 2% is found.

3 Flow and Heat Transfer Analysis

In this paper, control volume method is applied to analyze flow and heat transfer parameters with measured temperature and pressure data. As shown in Fig. 3, S1 and S2 are cross sections at the inlet and outlet of the control volume where the temperature and pressure are measured, and S3 is the inner wall surface of the test section. τ_w is the wall shear stress due to the skin friction on S3,

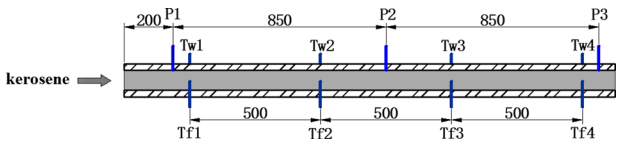

Fig. 2 Sketch of the test section with temperature and pressure measurements (unit: millimeter)

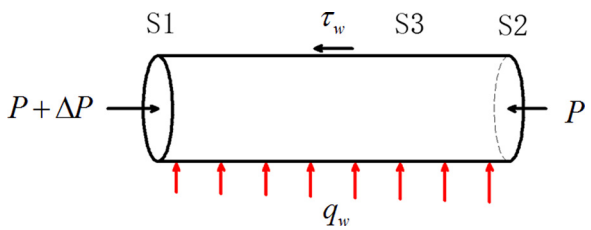

Fig. 3 Control volume for flow and heat transfer analysis

$P + \Delta P$ and P are the pressure forces applied on S1 and S2, and q_w is the heat flux through S3 into the control volume.

Since aviation kerosene is a complex mixture composed of hundreds of hydrocarbon components, a ten-species surrogate proposed by Zhong et al. [3] is used to determine viscosity, density, thermal conductivity, specific heat, and other properties of China RP-3 kerosene with the extended corresponding states model (ECS) [5]. Figures 4(*a*)–4(*c*) show the variations of kerosene density, specific internal energy, and specific enthalpy with temperature under supercritical pressures of 3 MPa and 4 MPa. The other properties of kerosene including thermal conductivity, viscosity, and specific heat can be found in our previous study [3].

3.1 Mass Conservation.

Mass conservation equation

$$\dot{m}_1 - \dot{m}_2 = \frac{d}{dt}\int_R \rho dV = \Delta V \frac{d\overline{\rho}}{dt} \tag{2}$$

where $\dot{m}_1$ and $\dot{m}_2$ are the mass flow rate through S1 and S2, for example, the inlet and outlet of test section; R is the control volume; $\Delta V = \pi d^2 l/4$ is the control volume; d is the inner diameter of the test section; l is the distance between S1 and S2; and $\overline{\rho}$ is the average density based on the mean temperature defined as $\overline{T}_f = 0.5(T_{fs1} + T_{fs2})$, where T_{fs1} and T_{fs2} are the fuel temperatures measured by type-K thermocouples.

During the experiments, the fuel mass flow rate at the outlet of the test section does not change, and the fuel temperatures decrease slightly with time. The unsteady term, $(\Delta V)d\overline{\rho}/dt$, on the right-hand side of Eq. (2) is very small compared to other terms and can be neglected. For example, for test 1 as listed in Table 1, the maximum value of unsteady term $(\Delta V)d\overline{\rho}/dt$ for control volume between inlet and outlet of the test section is about 0.45 g/s, the mass flow rate at the outlet is 29 g/s, and the ratio is less than 1.6%. Therefore, the mass flow rates at the inlet and outlet of test section are approximately equal, and the turbulent flow is stationary.

3.2 Momentum Conservation.

Axial momentum conservation equation

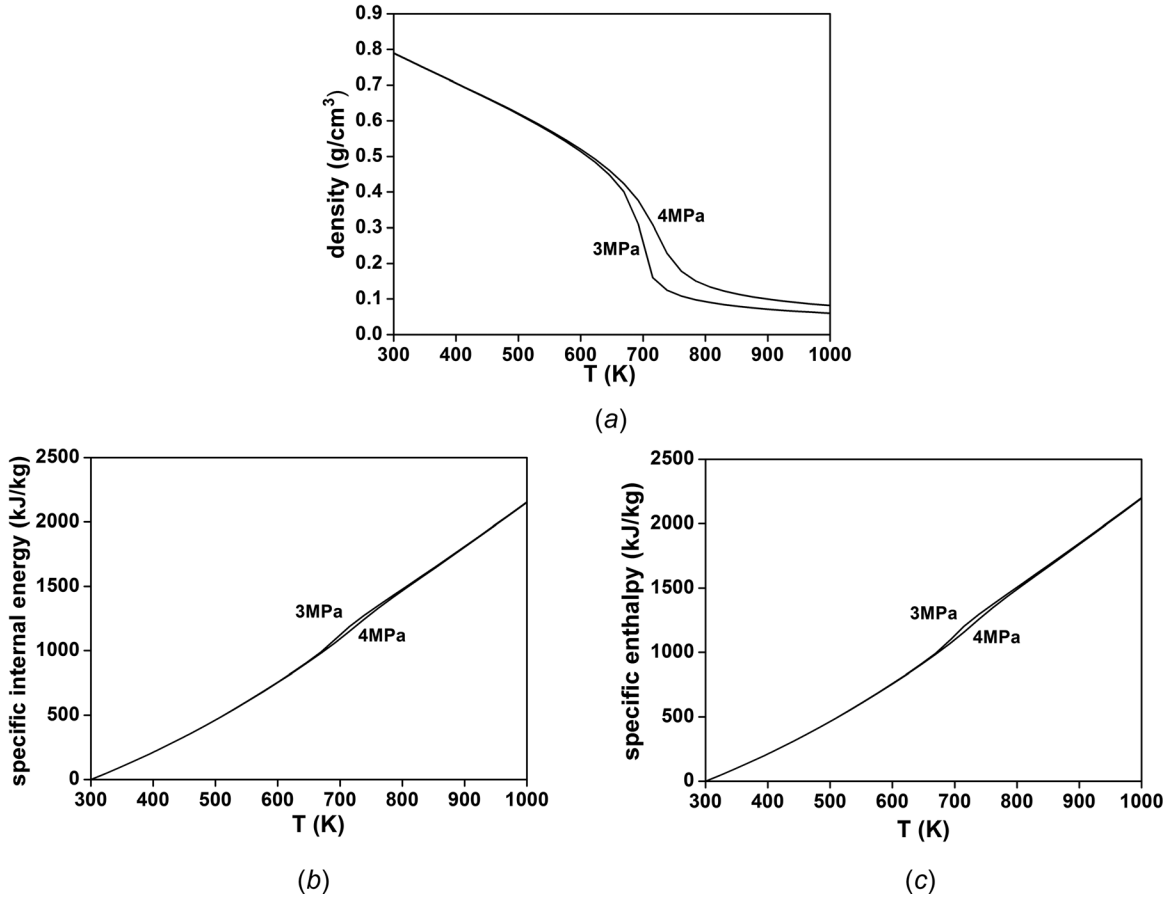

Fig. 4 (*a*) Variation of fuel density with temperature, (*b*) variation of fuel-specific internal energy with temperature, and (*c*) variation of fuel-specific enthalpy with temperature

Table 1 Summary of test section conditions

Test number	Inlet pressure (MPa)	Inlet temperature (K)	Wall heat flux (kW/m^2)	Mass flow rate (g/s)	Prandtl number
1	3.0	660	470	29	1.7–3.5
2	4.0	700	230	38	2.1–2.8
3	3.1	660	260	20	1.6–3.5
4	3.8	670	330	26	1.8–3.5

$$\sum F = \frac{d}{dt}\int_R \rho u dV + \int_{s_1+s_2+s_3} \rho u \mathbf{u}\cdot d\mathbf{S} = \Delta V \frac{d\overline{\rho u}}{dt} + (u_2\dot{m}_2 - u_1\dot{m}_1) \tag{3}$$

$$\sum F = \frac{\pi d^2 \Delta P}{4} - \pi d l \tau_w \tag{4}$$

where $\sum F$ denotes the forces acting on the control volume between P1 and P2, for example, including wall shear stress and pressure difference of the control volume; u_1 and u_2 are the fuel velocity at the cross section of S1 and S2 which can be determined by fuel mass flow rate and fuel density; the average velocity $\overline{u}$ is calculated by fuel mass flow rate and the average density $\overline{\rho}$; and ΔP is measured by the high-resolution differential pressure sensor. In our experiments, the flow reaches a quasi-steady state, and the unsteady term of Eq. (3) can be neglected. C_f is calculated with the formula of $\tau_w = (1/L)\int_0^L 0.5 C_f \rho u^2 dx = 0.5 C_f \overline{\rho u^2}$, and it is an average value on the surface of S3 according to Fig. 3 and the control volume analysis.

3.3 Energy Conservation. Energy conservation equation

$$\overline{q}_w A = \frac{d}{dt}\int_R \rho e dV + \int_{s_1+s_2} \rho(e + p/\rho)\mathbf{u}\cdot d\mathbf{S} + \left(\frac{d}{dt}\int_R \frac{1}{2}\rho \mathbf{u}\cdot\mathbf{u} dV + \int_{s_1+s_2}\left(\frac{1}{2}\rho \mathbf{u}\cdot\mathbf{u}\right)\mathbf{u}\cdot d\mathbf{S}\right) - \left(\int_{S_2} k\frac{\partial T}{\partial x}\cdot dS - \int_{S_1} k\frac{\partial T}{\partial x}\cdot dS\right) \tag{5}$$

$$\rightarrow \quad \overline{q}_w A = \Delta V \frac{d(\overline{\rho e})}{dt} + \int_{s_1+s_2} \rho h \mathbf{u}\cdot d\mathbf{S} = \Delta V \frac{d(\overline{\rho e})}{dt} + (h_2\dot{m}_2 - h_1\dot{m}_1) \tag{6}$$

where $\overline{q}_w$ is the average wall heat flux through S3 between Tf1 and Tf2, for example; $A = \pi d l$ is the area of S3; ρ is the fuel density; e is the internal energy per unit mass; and h is the enthalpy per unit mass. The third and fourth terms on the right-hand side of Eq. (5) are fuel kinetic energy term and heat conduction term through surfaces S1 and S2, respectively. The heat conduction

term can be estimated using the fuel temperature and fuel thermal conductivity at measurement locations. The fuel kinetic energy term and heat conduction term are neglected due to very small values compared to other terms on the right-hand side of Eq. (5). For example, in test 1 of Table 1, the values of fuel kinetic energy term and heat conduction term are smaller than 0.5 W and 0.0001 W, respectively, which are negligible compared to the values of the first and second terms on the right-hand side of Eq. (5) of about 360 W and 4300 W. The work done by the viscous forces on S3 is zero due to the stationary tube wall, and the work done by viscous forces on the cross sections of S1 and S2 are neglected compared to that done by pressure. The fuel internal energy and enthalpy per unit mass can be determined with measured fuel temperature and pressure. The term $d(\overline{\rho e})/dt$ is determined by calculating the difference of $(\overline{\rho e})$ at two instants of time with a time internal of 0.5 s during the test, and the order of the error caused by this difference approximation is less than 6% compared to the exact value of $\Delta V(d(\overline{\rho e})/dt)$. At last, the average heat flux through S3 can be determined via Eq. (6). With the wall heat flux and the inner wall temperature of the test section obtained by one-dimensional heat conduction analysis described in Ref. [10], heat transfer coefficient may be calculated by $\lambda = \overline{q}_w/(\overline{T}_w - \overline{T}_f)$ as well as Nusselt number $\mathrm{Nu} = \lambda d/k$.

4 Results and Discussion

4.1 Reliability of the Experimental Data. Before kerosene experiments, reliability of the heating facility and measurements as well as the control volume analysis method was examined via experiments of flow and heat transfer of nitrogen. The skin friction coefficient and Nusselt number of nitrogen were compared with the results obtained by the classical formula of Sider–Tate correlation [8] ($\mathrm{Nu} = 0.027\mathrm{Re}^{0.8}\mathrm{Pr}^{1/3}(\mu_f/\mu_w)^{0.14}$) and Prandtl correlation ($C_f = 0.046\mathrm{Re}^{-0.2}$). Good agreements between the experimental results and theoretical values are found.

4.2 Flow and Heat Transfer Properties of Supercritical Kerosene. Table 1 lists test conditions of supercritical kerosene including inlet pressure, inlet temperature, wall heat flux, fuel mass flow rate, and the range of Prandtl number of fuel in the test section. Both the inlet pressure and temperature exceed the critical values (2.4 MPa and 640 K) to ensure that kerosene is at supercritical state. In our experiments, Reynolds number defined by the inner diameter of the test tube and fuel parameters exceeds 1×10^5, and the kerosene flow is fully turbulent. At the same time, buoyancy effects can be ignored since the values of $\mathrm{Gr}/\mathrm{Re}_d^2$ in the test section are smaller than 0.008, where Gr is the Grashof number.

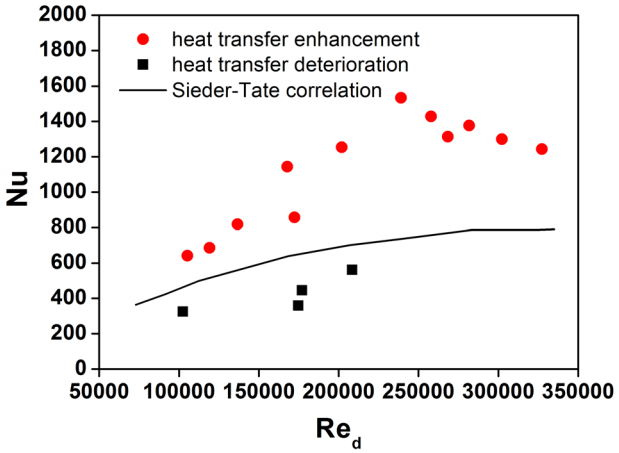

Fig. 6 Nusselt number versus Reynolds number

Figures 5(*a*) and 5(*b*) plot the time history of fuel pressure and temperature at the inlet and outlet of test section for test 1. The pressures at the inlet and the outlet remain constant after $t = 8$ s, which indicates that kerosene flow achieves a steady state. The inlet fuel temperature is kept at a constant value of 660 K after $t = 8$ s too. The temperature, pressure, pressure drop, and mass flow rate data acquired between $t = 8$ s and $t = 12$ s are used to calculate Nu and C_f through the control volume analysis. The outlet fuel temperature decreases at a rate of approximately 3–4 K/s because the heating power for the test section was turned off during experiments for a reliable measurement of wall temperatures.

Figure 6 shows the variation of the Nusselt number with changes in the Reynolds number. The dots are the experimental data, and the black line is the result of the classical Sider–Tate correlation. From Fig. 6, we can see that both heat transfer enhancement (the circular dots) and heat transfer deterioration (the black square dots) occurred in the experiments, which are caused by the significant variations in fuel thermophysical properties in the vicinity of the tube wall according to the conclusions of our previous study [11] rather than by Reynolds number.

Figure 7 gives the values of fuel and wall temperature corresponding to occurrences of heat transfer enhancement and deterioration. The dashed line and dotted line plotted in the figure indicate values of critical temperature (~640 K) and pseudocritical temperature (700 K). It is obvious in the figure that for heat transfer deterioration, fuel temperature is always lower than the pseudocritical value and the wall temperature is close or slightly

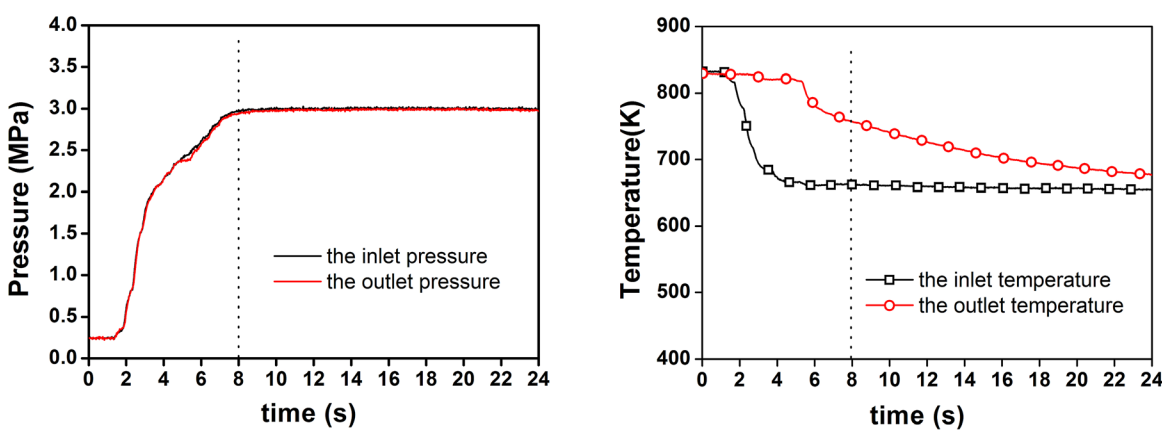

(*a*) (*b*)

Fig. 5 (*a*) Time history of inlet and outlet pressures for test 1 and (*b*) time history of inlet and outlet temperatures for test 1

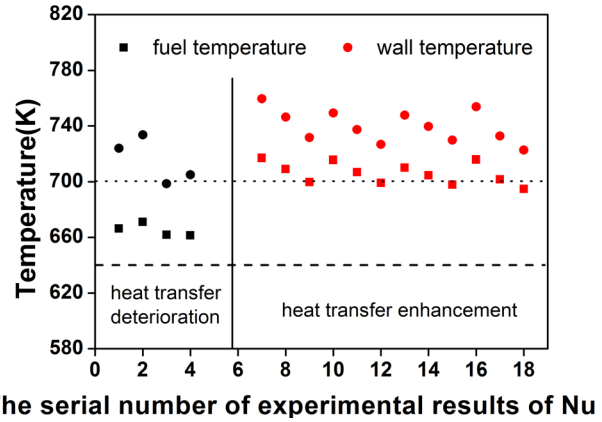

Fig. 7 The fuel and inner wall temperatures for different heat transfer phenomena

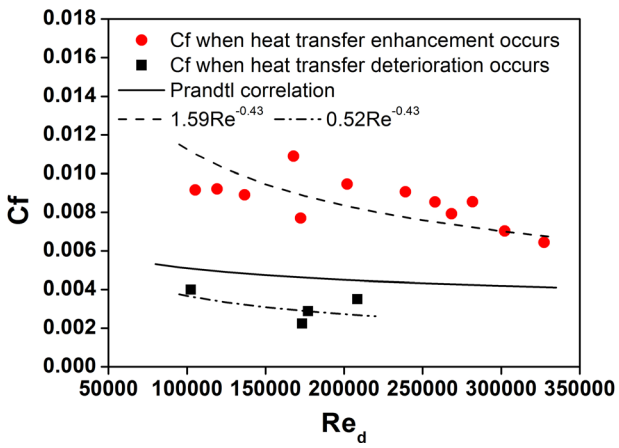

Fig. 8 Skin friction coefficient versus Reynolds number

higher than the pseudocritical value. As heat transfer enhancement occurs, fuel temperature is very close to or even slightly higher than the pseudocritical value. The present experimental results show that the occurrence of heat transfer enhancement or deterioration is related to the change of fuel temperature and wall temperature as they approach the critical and the pseudocritical values, which are consistent with that found in our numerical work [11].

Figure 8 plots the results of skin friction coefficient as a function of Reynolds number. The experimental data and the result of classical Prandtl correlation are both presented. It is found that the experimental value of C_f is smaller than that calculated by Prandtl correlation as heat transfer deterioration happens and it is larger than that of Prandtl correlation when heat transfer enhances. It indicates that the change of convective heat transfer is consistent with the change of skin friction for the present flow conditions. The correlations of skin friction coefficient with Reynolds number are developed, and the mathematical expressions are $1.59\mathrm{Re}^{-0.43}$ and $0.52\mathrm{Re}^{-0.43}$ for heat transfer enhancement and deterioration, respectively. Comparisons of results of the correlations and experimental data are shown in Fig. 8. It is found that the average standard deviation of the expressions for heat transfer enhancement and deterioration is 11% and 12%, respectively.

Figure 9 shows the experimental results of Nusselt number divided by $C_f\mathrm{Pr}^{1/3}$ as a function of Reynolds number. The Chilton–Colburn analogy relation of $0.5\mathrm{Re}_d$ is also plotted to examine its validity for supercritical kerosene flow. The experimental data agree quite well with the Chilton–Colburn analogy with an average deviation of 8%. The present experimental results show that the Chilton–Colburn analogy relation also applies to

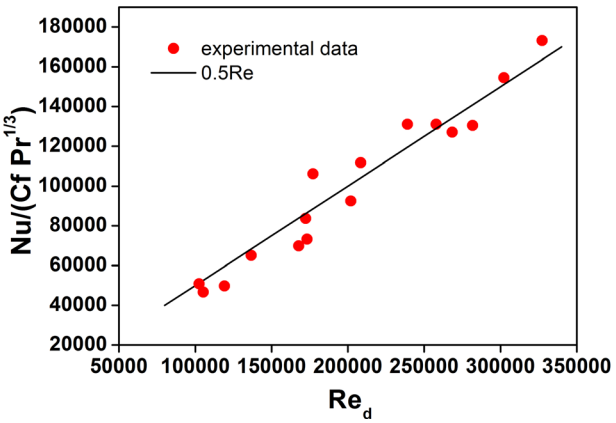

Fig. 9 Chilton–Colburn analogy of supercritical kerosene flow

turbulent flow and heat transfer of supercritical kerosene through horizontal straight circular tube. To the best of our knowledge, it is the first time that validity of the Chilton–Colburn analogy based on the idea of the Reynolds analogy relation is demonstrated and reported by experiments for turbulent flow of supercritical hydrocarbons.

5 Conclusions

In this paper, flow and heat transfer properties of supercritical China RP-3 kerosene through horizontal straight circular tube are studied experimentally. With measured data of fuel temperature and pressure, etc., distributions of Nusselt number and skin friction coefficient can be determined. Several conclusions may be obtained based on the present results.

(1) For turbulent flow of supercritical kerosene heat transfer, deterioration and enhancement occurred, which attributes to the variations of fuel thermophysical properties in the vicinity of the tube wall.
(2) It is found that the skin friction coefficient is smaller than the value of classical Prandtl correlation when heat transfer deterioration occurs and is larger than the correlation value when heat transfer enhancement happens.
(3) The Chilton–Colburn analogy is demonstrated to be valid for turbulent flow and heat transfer of supercritical kerosene through horizontal straight circular tube according to the present experimental data.

Acknowledgment

This work was funded by the Natural Science Foundation of China under Contract Nos. 11172309 and 91441102.

Nomenclature

A = area, m^2
C_f = skin friction coefficient
d = inner diameter of the test section, m
e = internal energy per unit mass, J/kg
Gr = Grashof number
h = enthalpy per unit mass, J/kg
k = thermal conductivity, W/m K
l = distance between S1 and S2, m
$\dot{m}$ = mass flow rate, kg/s
Nu = Nusselt number
P = pressure, Pa
Pr = Prandtl number
q_w = heat flux, $\mathrm{W/m}^2$
Re_d = Reynolds number defined by tube inner diameter

t = time, s
T = temperature, K
u = axial velocity, m/s
ΔP = pressure difference, Pa
ΔV = volume, m^3
λ = heat transfer coefficient, W/m^2 K
μ = dynamic viscosity, Pa s
ρ = density, kg/m^3
τ_w = wall shear stress, Pa

References

[1] Huang, H., Spadaccini, L. J., and Sobel, D. R., 2004, "Fuel Cooled Thermal Management for Advanced Aero-Engines," ASME J. Eng. Gas Turbines Power, **126**(2), pp. 284–293.

[2] Linne, D. L., and Meyer, M. L., 1997, "Evaluation of Heat Transfer and Thermal Stability of Supercritical JP-7 Fuel," AIAA Paper No. 97-3041.

[3] Zhong, F. Q., Fan, X. J., Yu, G., Li, J., and Sung, C.-J., 2009, "Heat Transfer of Aviation Kerosene at Supercritical Conditions," J. Thermophys. Heat Transfer, **23**(3), pp. 543–550.

[4] Zhong, F. Q., Fan, X. J., and Yu, G., 2011, "Thermal Cracking and Heat Sink Capacity of Aviation Kerosene Under Supercritical Conditions," J. Thermophys. Heat Transfer, **25**(3), pp. 450–456.

[5] Yang, V., 2000, "Modeling of Supercritical Vaporization, Mixing, and Combustion Processes in Liquid-Fueled Propulsion System," Proc. Combust. Inst., **28**(1), pp. 925–942.

[6] Liao, S. M., and Zhao, T. S., 2002, "Measurement of Heat Transfer Coefficients From Supercritical Carbon Dioxide Flowing in Horizontal Mini/Macro Channels," ASME J. Heat Transfer, **124**(3), pp. 413–420.

[7] Wang, Y. Z., Hua, Y. X., and Meng, H., 2010, "Numerical Studies of Supercritical Turbulent Convective Heat Transfer of Cryogenic-Propellant Methane," J. Thermophys. Heat Transfer, **24**(3), pp. 490–500.

[8] Sider, E. N., and Tate, C. E., 1936, "Heat Transfer and Pressure Drop of Liquids in Tubes," Ind. Eng. Chem., **28**(12), pp. 1429–1435.

[9] Colburn, A. P., 1964, "A Method of Correlating Forced Convection Heat Transfer Data and a Comparison With Fluid Friction," Int. J. Heat Mass Transfer, **7**(12), pp. 1359–1384.

[10] Meyer, M. L., 1995, "Electrically Heated Tube Investigation of Cooling Channel Geometry Effects," AIAA Paper No. 95-2500.

[11] Dang, G. X., Zhong, F. Q., Zhang, Y. J., and Zhang, X. Y., 2015, "Numerical Study of Heat Transfer Deterioration of Turbulent Supercritical Kerosene Flow in Heated Circular Tube," Int. J. Heat Mass Transfer, **85**, pp. 1003–1011.